13th International Symposium on Turbulence and Shear Flow Phenomena (TSFP13)
Montreal, Canada, June 25–28, 2024

# ATTENUATION MECHANISM OF WALL TURBULENCE BY HEAVY FINITE-SIZE PARTICLES

**Yutaro Motoori**
Graduate School of Engineering Science
Osaka University
1-3 Machikaneyama, Toyonaka, Osaka, 560-8531, Japan
y.motoori.es@osaka-u.ac.jp

**Susumu Goto**
Graduate School of Engineering Science
Osaka University
1-3 Machikaneyama, Toyonaka, Osaka, 560-8531, Japan
s.goto.es@osaka-u.ac.jp

## ABSTRACT

We conduct direct numerical simulations of turbulent channel flow laden with heavy finite-size solid particles to understand the physical mechanism of the modulation of wall turbulence. When particles cannot follow the swirling motion of wall-attached vortices, they cannot also follow the mean flow, thus creating shedding vortices around them. These shedding vortices produce additional energy dissipation, which reduces the turbulence energy production by the mean flow. Consequently, turbulent energy is attenuated. With the attenuation mechanism of wall turbulence, we can describe the necessary conditions for the attenuation. Moreover, we demonstrate that the degree of turbulence attenuation is determined by the energy dissipation rate around particles.

## INTRODUCTION

When we add solid particles into turbulent flow, turbulence intensity increases or decreases. Many experiments (Maeda *et al.*, 1980; Tsuji *et al.*, 1984; Gore & Crowe, 1989; Kulick *et al.*, 1994; Rogers & Eaton, 1991; Kussin & Sommerfeld, 2002) and direct numerical simulations (DNS) (Maeda *et al.*, 1980; Tsuji *et al.*, 1984; Gore & Crowe, 1989; Kulick *et al.*, 1994; Rogers & Eaton, 1991; Kussin & Sommerfeld, 2002) demonstrated that turbulent energy is attenuated with the addition of *small* particles. However, the physical mechanism of turbulence modulation by particles is not fully understood. This is because turbulence modulation depends on many parameters characterizing the interaction between particles and turbulence. For investigating such complicated phenomena, numerical simulations play an important role. Many authors (Ten Cate *et al.*, 2004; Burton & Eaton, 2005; Lucci *et al.*, 2010; Yeo *et al.*, 2010; Bellani *et al.*, 2012; Wang *et al.*, 2014; Schneiders *et al.*, 2017; Uhlmann & Chouippe, 2017; Oka & Goto, 2022; Shen *et al.*, 2022; Peng *et al.*, 2023) conducted DNS, under periodic boundary conditions, to explore the effects of finite-size spherical particles on turbulence modulation. Recently, our group (Oka & Goto, 2022) also conducted DNS of particles-laden periodic turbulence. In the study, they derived a formula describing the degree of turbulence attenuation rate on the basis of the physical picture of the turbulence attenuation. Balachandar *et al.* (2024) further developed this picture to construct the subgrid model for particle-turbulence interactions.

Although the pioneering studies on turbulence modulation by particles were experiments (Tsuji & Morikawa, 1982; Tsuji *et al.*, 1984; Kulick *et al.*, 1994) of turbulence between a pair of parallel planes, the progress in understanding wall turbulence modulation is behind periodic turbulence, which is considered as turbulence far from walls. Kulick *et al.* (1994) demonstrated that the turbulence intensity decreased more significantly with the addition of heavy copper particles than lighter glass ones. They concluded that, as the relaxation time $\tau_p$ of particles is longer than the time scale $\tau_f$ of fluid motion, the turbulence is attenuated more significantly. This means that when the Stokes number $St(=\tau_p/\tau_f)$ is larger, the turbulence is more attenuated. Note that the relaxation time is longer for heavier particles if the particles have the same diameter. Similar Stokes-number dependence on the turbulence modulation was also shown by DNS (Dritselis & Vlachos, 2008, 2011; Lee *et al.*, 2015; Wang & Richter, 2019; Zhou *et al.*, 2020) of turbulent channel flow interacting with suspended pointwise particles. In addition, although DNS studies (Kajishima *et al.*, 2001; Uhlmann, 2008; Zeng *et al.*, 2008; Shao *et al.*, 2012; Fornari *et al.*, 2016; Wang *et al.*, 2016; Yu *et al.*, 2017; Peng *et al.*, 2019; Costa *et al.*, 2020; Muramulla *et al.*, 2020; Yu *et al.*, 2021; Xia *et al.*, 2021; Costa *et al.*, 2021) of turbulent channel flow with finite-size particles were also carried out, a physical picture of wall turbulence modulation is still unclear. In most of these DNS, the friction Reynolds number is about 180. Therefore, although there are pieces of knowledge about turbulence modulation in the buffer layer, the knowledge in the outer layer is limited.

The purpose of the present study is to reveal the physical mechanism of wall turbulence modulation including from the buffer to outer layers. To this end, we conduct the DNS of turbulent channel flow laden with finite-size spherical particles. We change the three parameters: the diameter, mass density and friction Reynolds number $Re_\tau$. Although the logarithmic layer is limited even for the highest $Re_\tau(=512)$ of our DNS,

there is a scale separation between the buffer and outer layers. In the present study, we focus on these two layers. Based on the results obtained by the DNS, we propose the modulation mechanism of wall turbulence. This mechanism enables us to describe the necessary conditions for turbulence attenuation and the degree of the attenuation in the buffer and outer layers.

## DIRECT NUMERICAL SIMULATIONS

We conduct the DNS of particles-laden turbulence driven in two parallel walls. The flow obeys the Navier–Stokes equation for an incompressible fluid. The particles are governed by the equations of motion for translation and rotation of a sphere. To evaluate the interaction between fluid and particles, we use an immersed boundary method proposed by Breugem (2012). For the spatial discretization of the terms in the governing equations, we use a standard finite difference method. The temporal integrations of the viscous and convection terms are made by using the second-order Crank–Nicolson method and the three-step Runge–Kutta method, respectively. The detailed numerical simulation method is the same as in Breugem (2012).

In the present study, we simulate turbulence for the four friction Reynolds numbers: $Re_\tau = u_\tau h/\nu = 512$, 360, 256 and 180 (where $u_\tau$ is the friction velocity, $h$ is the channel half-width and $\nu$ is the kinematic viscosity). Then, we add particles to the turbulence. The particles are characterised by three parameters: the diameter $D$, the mass density $\rho_p$ and the number $N_p$ of the added particles. Fixing a small volume fraction $\Lambda = 0.0082$ of particles, we change $D$ and $\rho_p$. We set the particle diameter as $D^+ = 16$, 32 and 64 for $Re_\tau = 512$, $D^+ = 16$ and 32 for $Re_\tau = 360$ and 256, and $D^+ = 16$ for $Re_\tau = 180$. Here, $\cdot^+$ denotes the quantity normalized by $u_\tau$ and $\nu$. All particles are ten times smaller than the channel half-width ($D/h \leq 0.13$). We set the mass density $\rho_p$ larger than that $\rho_f$ of the fluid: $\rho_p/\rho_f = 2$, 8, 32 and 128.

In the following analyses, instead of $\rho_p/\rho_f$, we show results by using the two Stokes numbers: $St_h = \tau_p/\tau_h$, which is defined as the ratio of the particle relaxation time $\tau_p (= \rho_p D^2/(18\rho_f \nu))$ to the eddy turnover time $\tau_h = h/u_\tau$ of the wall-attached vortices in the outer layer, and $St_+ = \tau_p/\tau_+$, which is defined as the ratio of $\tau_p$ to the wall viscous time $\tau_+ (= \nu/u_\tau^2)$. When $St_h$ is less than 1, the particles can follow the swirling motion induced by the outer-layer vortices ($\sim h$); otherwise, they cannot follow the swirls. The range of $St_h$ examined in the present study is $St_h = 0.056$–57. On the other hand, the shortest relaxation time ($St_+ = 28$) among the simulated particles is comparable to the time scale of buffer-layer vortices (Soldati & Marchioli, 2009). In other words, none of the simulated particles can thoroughly follow the swirl of these vortices. In the following, we show results in the statistically steady state after adding the particles.

## RESULTS

### Modulation of vortices

First, let us examine the modulation of coherent vortices in turbulence at $Re_\tau = 512$. Figure 1 shows vortices in turbulence laden with the smallest ($D/h = 0.031$, i.e. $D^+ = 16$) particles. The Stokes numbers differ between the panels (a) $St_h = 0.056$ ($St_+ = 28$) and (b) $St_h = 3.6$ ($St_+ = 1820$). The gray objects are the isosurfaces of the second invariant $Q$ of the velocity gradient tensor. Since the velocity gradient in turbulence is determined by the smallest-scale structures, the positive isosurfaces of $Q$ capture only the smallest-scale vortices

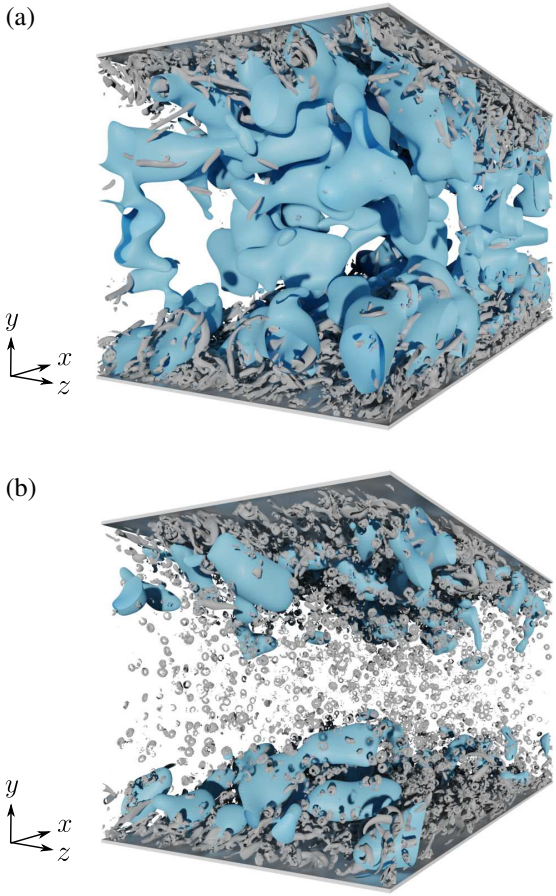


Figure 1. Visualisations of the modulation of coherent vortices in turbulence at $Re_\tau = 512$ due to particles with the same diameter ($D/h = 0.031$, i.e. $D^+ = 16$) but different Stokes number: (a) $St_h = 0.056$ ($St_+ = 28$) and (b) $St_h = 3.6$ ($St_+ = 1820$). The gray vortices are identified by the positive isosurfaces of the second invariant $Q$ of the velocity gradient tensor. The blue vortices are identified by the second invariant $\widetilde{Q}^{(\ell)}$ of the velocity gradient tensor coarse-grained at $\ell = 0.2h$. We set the thresholds as $Q^+ = 7.0 \times 10^{-3}$ and $\widetilde{Q}^{(\ell)+} = 3.0 \times 10^{-5}$.

(Motoori & Goto, 2019, 2021). Therefore, to extract larger-scale vortices, we apply the three-dimensional Gaussian filter (Motoori & Goto, 2019) with filter width $\ell$ to the fluctuation velocity. We then evaluate the second invariant $\widetilde{Q}^{(\ell)}$ of the velocity gradient tensor coarse-grained at $\ell = 0.2h$ to identify the channel-half-width-scale vortices (blue objects), i.e. wall-attached vortices developing in the outer layer. We can see in panel (a) that the blue outer-layer vortices are developed even in the presence of particles with $St_h = 0.056$; whereas, in panel (b), these vortices are attenuated due to particles with $St_h = 3.6$.

It is also important to see that, when turbulence attenuation occurs, vortices are shed from particles. Figure 2 shows the magnification of subdomains in figure 1. Here, we visualize particles by the white surfaces. Panels (a) and (b–i) correspond to the buffer layer, whereas panel (b–ii) does the outer layer. Since $St_h (= 3.6)$ of the particles shown in figure 2(b) is larger than unity, they cannot follow the swirling motion of the outer-layer vortices, and therefore they cannot also follow the mean flow in the outer layer. This velocity difference between the particles and fluid in the streamwise direction causes the creation of vortex rings around particles (figure 2b–ii). In

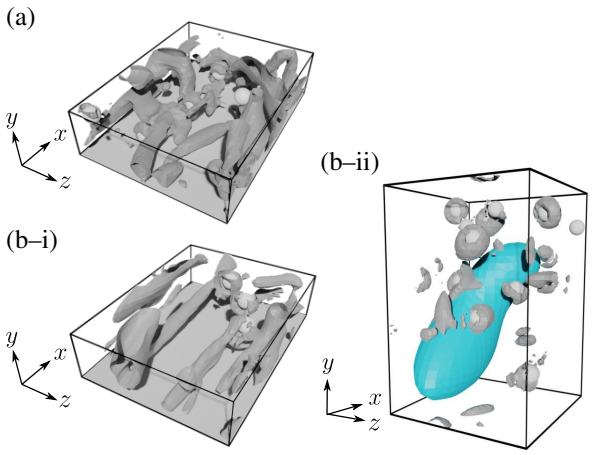


Figure 2. Magnification of subdomains in figures 1(a) and (b). (a,b–i) $0 \le y^+ \le 50$ and (b–ii) $0.3 \le y/h \le 0.75$ (i.e. $154 \le y^+ \le 384$). Particles are depicted by the white surfaces.

addition, since the buffer-layer vortices swirl faster than the outer-layer ones, the particles cannot also follow the mean flow in the buffer layer. Thus, vortex rings are also created in this layer (figure 2b–i).

On the other hand, particles with $St_h = 0.056$ (figures 1a and 2a) can follow the outer-layer vortices. Therefore, we cannot observe the shedding vortices in the outer-layer. However, $St_+$ of these particles is 28, which means that they cannot follow the vortices and mean flow in the buffer layer. Therefore, the shedding vortices are created around some particles (figure 2a), though it is less obvious than in the case of figure 2(b–i) due to the smallness of $St_+$.

The above visualizations provide the clear evidence that when particles cannot follow the wall-attached vortices, and therefore the mean flow, the shedding vortices can be created. These vortices are important for turbulence attenuation because they produce energy dissipation, which may reduce the energy production from the mean flow to wall-attached vortices. In the next subsection, we quantitatively discuss the turbulence attenuation.

### Turbulent energy

We show in figure 3 the wall-normal profile of the turbulent kinetic energy $K(y)$ averaged in the homogeneous direction and time for $Re_\tau = 512$. The blue dashed line shows the value $K_\times(y)$ for the single-phase flow. Panel (a) shows the Stokes-number-dependence (lighter thicker lines imply larger Stokes numbers) for the smallest particles ($D/h = 0.031$). We see that for larger Stokes numbers, the turbulent energy is attenuated more significantly at any height. More precisely, it decreases from the near-wall region, and the outer-layer turbulence gets attenuated for $St_h \gtrsim 1$. For example, particles with $St_h = 0.056$, namely, $St_+ = 28$ attenuate turbulence only for $y/h \lesssim 0.1$ (i.e. $y^+ \lesssim 50$). This is because these particles cannot follow the buffer-layer vortices. On the other hand, those with $St_h = 0.89$ attenuate turbulence at any height. These quantitative results are consistent with the observations in figures 1 and 2. We can also see similar Stokes-number dependences in the inset of figure 3(a), which shows the results for $Re_\tau = 180$.

Next, we show in figure 3(b) the results for a fixed $St_h$(= 3.6) but different $D/h$ (lighter thicker lines imply smaller particles). Since these particles satisfy $St_h \gtrsim 1$, turbulent energy can be attenuated at any height. It is important to observe that its degree is larger for smaller $D$. This is because smaller particles can produce larger energy dissipation rate.

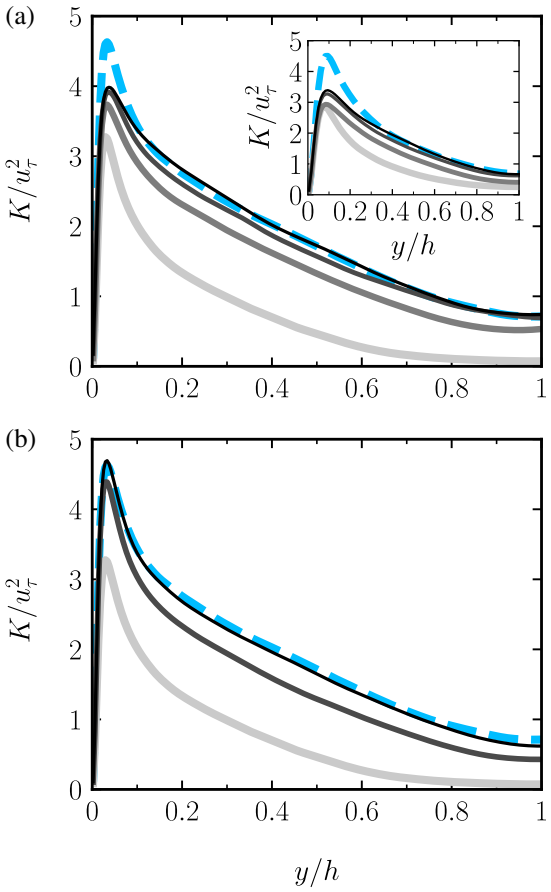


Figure 3. Wall-normal profile of the mean turbulent kinetic energy $K$ for $Re_\tau = 512$. (a) Stokes-number dependence [$St_h = 0.056$ (black), 0.22 (dark gray), 0.89 (light gray) and 3.6 (very light gray)] for the particle diameter $D/h = 0.031$. (b) Particle-diameter dependence [$D/h = 0.031$ (black), 0.063 (gray) and 0.13 (light gray)] for the Stokes number $St_h = 3.6$. The blue dashed line shows the result for the single-phase flow. The inset in (a) shows the results for $Re_\tau = 180$ and $St_h = 0.016$ (black), 0.63 (dark gray), 2.5 (light gray) and 10 (very light gray).

## DISCUSSIONS

### Attenuation mechanism of wall turbulence

We describe the attenuation mechanism of wall turbulence based on the results shown in the previous section. When the relaxation time of particles existing at a height $y_p$ is longer than the turnover time of the wall-attached vortices with the size $\ell \approx y_p$, these particles are not capable of following the vortices and the mean flow around $y_p$. Then, when the particle Reynolds number based on the relative velocity is sufficiently larger than unity, vortices are shed around the particles (figures 1 and 2). These shedding vortices are sustained by acquiring a part of the energy from the mean flow and then dissipating around the particles. This additional energy dissipation rate $\varepsilon_p$ reduces the energy production rate due to the mean flow. Consequently, the turbulence is attenuated around $y_p$.

In the following, with this mechanism, we discuss the necessary conditions for turbulence attenuation, and we demonstrate that we can estimate the degree of turbulence attenuation in each of the buffer and outer layers.

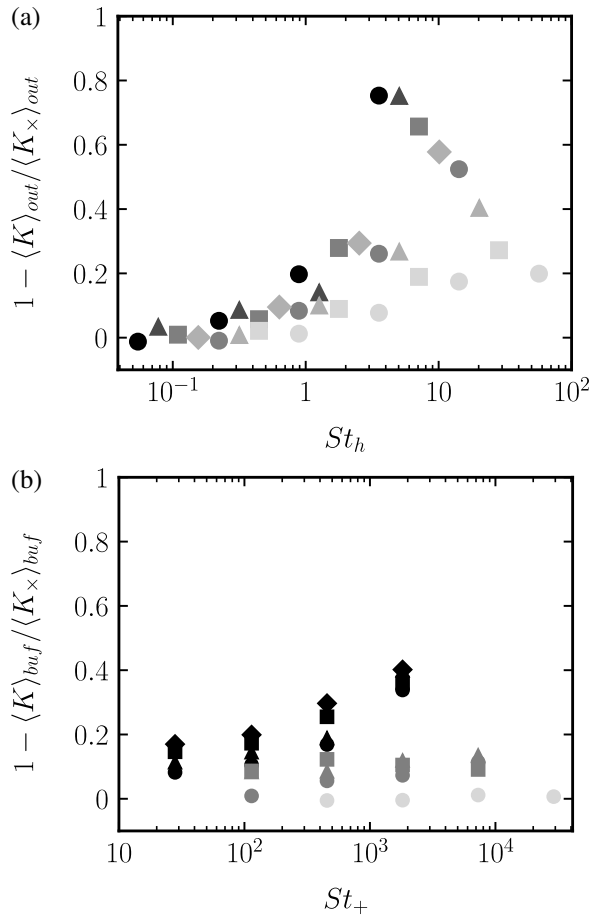


Figure 4. Attenuation rate of the turbulent kinetic energy in the (a) outer and (b) buffer layers, as functions of (a) $St_h$ and (b) $St_+$, respectively, for $Re_\tau = 512$ (circles), 360 (triangles), 256 (squares) and 180 (diamonds). The color of the symbols represents (a) $D/h$ and (b) $D^+$ (small particles for darker symbols).

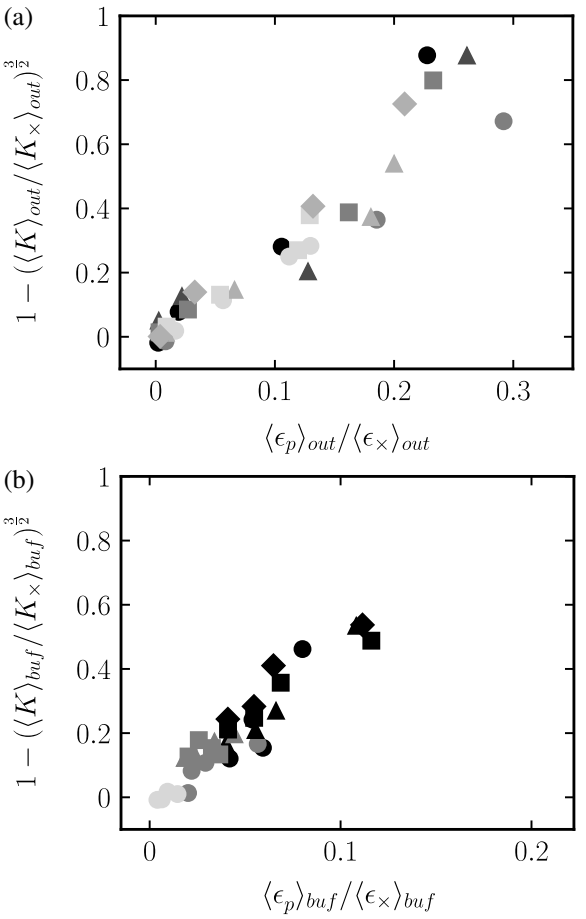


Figure 5. Numerical verification of (2) in the (a) outer and (b) buffer layers, as functions of $\varepsilon_p$ averaged in each layer, for $Re_\tau = 512$ (circles), 360 (triangles), 256 (squares) and 180 (diamonds). The color of the symbols represent (a) $D/h$ and (b) $D^+$ (small particles for darker symbols).

## Necessary condition for turbulence attenuation

Significant turbulence attenuation requires a large relative velocity between particles and fluid. Therefore, $St_h \gtrsim 1$ is necessary in the outer layer, while $St_+ \gtrsim 10$ is necessary in the buffer layer since the turnover time of the buffer-layer vortices is about ten times as large as $\tau_+$. To quantitatively show this, we define the buffer layer, including the viscous sublayer, as the height for $0 \le y^+ \le 50$, and the outer layer as for $0.3 \le y/h \le 1$. Then, we take the averages of kinetic energy for each of these two layers, denoted by $\langle K\rangle_{out}$ and $\langle K\rangle_{buf}$, and plot their attenuation rates in figure 4. Here, we show all results ($Re_\tau = 512$–$180$ and $D^+ = 16$–$64$) for (a) the outer and (b) buffer layers as functions of (a) $St_h$ and (b) $St_+$, respectively. We observe that in the outer layer, the turbulence attenuation rate increases for $St_h \gtrsim 1$. On the other hand, in the buffer layer, turbulence gets attenuated when $St_+$ is larger than 10. Note that the smallness of particles is also important for turbulence attenuation because smaller particles can produce energy dissipation more effectively. This explains that particles with $D^+ = 64$ (the lightest circles) as large as the buffer layer thickness cannot attenuate turbulence even if $St_+$ is large.

## Estimation of turbulence attenuation rate

Next, we estimate the degree of turbulence attenuation. Since the additional energy dissipation rate $\varepsilon_p$ around particles reduces the energy production rate from the mean flow, the attenuation degree can be described by $\varepsilon_p$. Recently, Oka & Goto (2022) derived a formula

$$1-\left(\frac{1}{1+\alpha_\times}\frac{\langle K\rangle}{\langle K_\times\rangle}\right)^{\frac{3}{2}} \propto \frac{\langle\varepsilon_p\rangle}{\langle\varepsilon_\times\rangle} \tag{1}$$

for estimating the turbulence attenuation rate in periodic turbulence. Here, $\langle\cdot\rangle$ denotes the average in the homogeneous direction and time, $\alpha_\times$ is the ratio between the mean and fluctuation energies for the single-phase flow, and $\varepsilon_\times$ the turbulent energy dissipation rate for the single-phase flow. Oka & Goto (2022) demonstrated that the degree of turbulence attenuation is determined by $\varepsilon_p$ by using their DNS results in periodic turbulence. We can derive the formula expressed by (1) under the assumption that the turbulent energy cascade is bypassed by particles. In the case of wall turbulence, if we assume that particles bypass the energy production from the mean flow and $\alpha_\times = 0$, we can obtain

$$1-\left(\frac{\langle K\rangle}{\langle K_\times\rangle}\right)^{\frac{3}{2}} \propto \frac{\langle\varepsilon_p\rangle}{\langle\varepsilon_\times\rangle}. \tag{2}$$

This formula can approximate the turbulence attenuation rate in the buffer and outer layers. Evidence is shown in figure 5. Here, we take the average of both hands of (2) for each of the

buffer and outer layers, and we plot all results according to (2). The numerical results demonstrate that, for each layer, the left-hand side of (2) is well proportional to the average of $\varepsilon_p/\varepsilon_\times$ irrespective of the particle properties and $Re_\tau$.

Incidentally, we use the relative velocity $\Delta u$ around particles and their surrounding fluid to evaluate $\varepsilon_p(=\Lambda|\Delta u|^3/D)$ in the outer layer. Our numerical results show that the relative velocity is well described by a formula (Balachandar, 2009) derived by assuming pointwise particles (figures are omitted). By using this, we can predict the turbulence attenuation rate in the outer layer solely from particle properties without evaluating $\varepsilon_p$. On the other hand, in the buffer layer, the estimated fluid velocity around particles has no physical meaning because $D$ is comparable to their existing height. Therefore, for the evaluation of $\varepsilon_p$ in the buffer layer, we take the local average for the energy dissipation rate in the spherical shell around particles.

## CONCLUSIONS

We have investigated the attenuation of wall turbulence due to solid particles by conducting DNS of turbulent channel flow laden with heavy finite-size particles. In the DNS, we change the particle diameter ($D/h = 0.031$–$0.13$), mass density ($\rho_p/\rho_f = 2$–$128$) and turbulence Reynolds number ($Re_\tau = 180$–$512$). With the obtained results, we reveal the attenuation mechanism of wall turbulence.

For the attenuation of turbulent energy, the shedding vortices created due to the velocity difference between particles and mean flow are important (figures 1 and 2), because they produce the additional energy dissipation rate $\varepsilon_p$. More concretely, the shedding vortices at a height $y_p$ are sustained by acquiring a part of the energy from the mean flow, then dissipating it around $y_p$. As a results, the energy production rate due to the mean flow is reduced by the amount of $\varepsilon_p$, and therefore turbulent energy is attenuated around $y_p$. This is the fundamental mechanism of the wall turbulence attenuation.

This physical picture of the turbulence attenuation due to the shedding vortices leads to the necessary conditions for turbulence attenuation. For the generation of the shedding vortices, the particle Reynolds number must be larger; therefore, the largeness of the Stokes number is necessary. However, note that the characteristic time scale of wall turbulence depends on the distance from the wall. Specifically, for a given height $y$, the wall-attached vortices with a size comparable to the height (i.e. $\ell \approx y$) have the longest turnover time. This explains the reason why the necessary conditions for turbulence attenuation in the outer and buffer layers are described in terms of $St_h \gtrsim 1$ and $St_+ \gtrsim 10$, respectively (figure 4).

We also demonstrate that the formula (2), which was originally derived as (1) by Oka & Goto (2022), is a good approximation even for estimating the turbulence attenuation rate in the outer and buffer layers (figure 5). This may imply that turbulence attenuation rate is locally determined by the energy dissipation rate $\varepsilon_p$ around particles. In developed turbulence, $\varepsilon_p$ is larger for smaller diameters and larger Stokes numbers. This explains the behavior of the degree of turbulence attenuation rate (figure 4). In this conference, we will develop the argument on the reason why (2) is valid for each layer of wall turbulence.

## ACKNOWLEDGEMENTS

This study was partly supported by the JSPS Grants-in-Aid for Scientific Research 20H02068 and 23K13253. The DNS were conducted by using the computational resources of the supercomputers Fugaku through the HPCI System Research Projects (hp220232 and hp230288). The numerical analyses were conducted under the auspices of the NIFS Collaboration Research Program (NIFS22KISS010 and NIFS24KISC007).

## REFERENCES

Balachandar, S. 2009 A scaling analysis for point-particle approaches to turbulent multiphase flows. *International Journal of Multiphase Flow* **35**, 801–810.

Balachandar, S., Peng, C. & Wang, L. P. 2024 Turbulence modulation by suspended finite-sized particles: Toward physics-based multiphase subgrid modeling. *Physical Review Fluids*, **9**, 044304.

Bellani, G., Byron, M. L., Collignon, A. G., Meyer, C. R. & Variano, E. A. 2012 Shape effects on turbulent modulation by large nearly neutrally buoyant particles. *Journal of Fluid Mechanics* **712**, 41–60.

Breugem, W. P. 2012 A second-order accurate immersed boundary method for fully resolved simulations of particle-laden flows. *Journal of Computational Physics* **231**, 4469–4498.

Burton, T. M. & Eaton, J. K. 2005 Fully resolved simulations of particle-turbulence interaction. *Journal of Fluid Mechanics* **545**, 67–111.

Costa, P., Brandt, L. & Picano, F. 2020 Interface-resolved simulations of small inertial particles in turbulent channel flow. *Journal of Fluid Mechanics* **883**, A54.

Costa, P., Brandt, L. & Picano, F. 2021 Near-wall turbulence modulation by small inertial particles. *Journal of Fluid Mechanics* **922**, A9.

Dritselis, C. D. & Vlachos, N. S. 2008 Numerical study of educed coherent structures in the near-wall region of a particle-laden channel flow. *Physics of Fluids* **20**, 055103.

Dritselis, C. D. & Vlachos, N. S. 2011 Numerical investigation of momentum exchange between particles and coherent structures in low Re turbulent channel flow. *Physics of Fluids* **23**, 025103.

Fornari, W., Formenti, A., Picano, F. & Brandt, L. 2016 The effect of particle density in turbulent channel flow laden with finite size particles in semi-dilute conditions. *Physics of Fluids* **28**, 033301.

Gore, R A & Crowe, C T 1989 Effect of particle size on modulating turbulent intensity. *International Journal of Multiphase Flow* **15**, 279–285.

Kajishima, T., Takiguchi, S., Hamasaki, H. & Miyake, Y. 2001 Turbulence structure of particle-laden flow in a vertical plane channel due to vortex shedding. *JSME International Journal Series B Fluids and Thermal Engineering* **44**, 526–535.

Kulick, J. D., Fessler, J. R. & Eaton, J. K. 1994 Particle response and turbulence modification in fully developed channel flow. *Journal of Fluid Mechanics* **277**, 109–134.

Kussin, J. & Sommerfeld, M. 2002 Experimental studies on particle behaviour and turbulence modification in horizontal channel flow with different wall roughness. *Experiments in Fluids* **33**, 143–159.

Lee, J., Ahn, J. & Sung, H. J. 2015 Comparison of large- and very-large-scale motions in turbulent pipe and channel flows. *Physics of Fluids* **27**, 025101.

Lucci, F., Ferrante, A. & Elghobashi, S. 2010 Modulation of isotropic turbulence by particles of Taylor length-scale size. *Journal of Fluid Mechanics* **650**, 5–55.

Maeda, M., Hishida, K. & Furutani, T. 1980 Velocity distri-

butions of air-solids suspension in upward pipe flow: effect of particles on air velocity distribution. *the Japan Society of Mechanical Engineers, Series B* **46**, 2313–2320.

Motoori, Y. & Goto, S. 2019 Generation mechanism of a hierarchy of vortices in a turbulent boundary layer. *Journal of Fluid Mechanics* **865**, 1085–1109.

Motoori, Y. & Goto, S. 2021 Hierarchy of coherent structures and real-space energy transfer in turbulent channel flow. *Journal of Fluid Mechanics* **911**, A27.

Muramulla, P., Tyagi, A., Goswami, P. S. & Kumaran, V. 2020 Disruption of turbulence due to particle loading in a dilute gas-particle suspension. *Journal of Fluid Mechanics* **889**, A28.

Oka, S. & Goto, S. 2022 Attenuation of turbulence in a periodic cube by finite-size spherical solid particles. *Journal of Fluid Mechanics* **949**, A45.

Peng, C., Ayala, O. M. & Wang, L. P. 2019 Flow modulation by a few fixed spherical particles in a turbulent channel flow. *Journal of Fluid Mechanics* **884**, A15.

Peng, C., Sun, Q. & Wang, L. P. 2023 Parameterization of turbulence modulation by finite-size solid particles in forced homogeneous isotropic turbulence. *Journal of Fluid Mechanics* **963**, A6.

Rogers, C. B. & Eaton, J. K. 1991 The effect of small particles on fluid turbulence in a flat-plate, turbulent boundary layer in air. *Physics of Fluids A* **3**, 928–937.

Schneiders, L., Meinke, M. & Schröder, W. 2017 Direct particle-fluid simulation of Kolmogorov-length-scale size particles in decaying isotropic turbulence. *Journal of Fluid Mechanics* **819**, 188–227.

Shao, X., Wu, T. & Yu, Z. 2012 Fully resolved numerical simulation of particle-laden turbulent flow in a horizontal channel at a low Reynolds number. *Journal of Fluid Mechanics* **693**, 319–344.

Shen, J., Peng, C., Wu, J., C., Kai L., Lu, Z. & Wang, L. P. 2022 Turbulence modulation by finite-size particles of different diameters and particle–fluid density ratios in homogeneous isotropic turbulence. *Journal of Turbulence* **23**, 433–453.

Soldati, A. & Marchioli, C. 2009 Physics and modelling of turbulent particle deposition and entrainment: Review of a systematic study. *International Journal of Multiphase Flow* **35**, 827–839.

Ten Cate, A., Derksen, J. J., Portela, L. M. & Van den Akker, H. E. 2004 Fully resolved simulations of colliding monodisperse spheres in forced isotropic turbulence. *Journal of Fluid Mechanics* **519**, 233–271.

Tsuji, Y. & Morikawa, Y. 1982 LDV measurements of an air-solid two-phase flow in a horizontal pipe. *Journal of Fluid Mechanics* **120**, 385–409.

Tsuji, Y., Morikawa, Y. & Shiomi, H. 1984 LDV measurements of an air-solid two-phase flow in a vertical pipe. *Journal of Fluid Mechanics* **139**, 417–434.

Uhlmann, M. 2008 Interface-resolved direct numerical simulation of vertical particulate channel flow in the turbulent regime. *Physics of Fluids* **20**, 053305.

Uhlmann, M. & Chouippe, A. 2017 Clustering and preferential concentration of finite-size particles in forced homogeneous-isotropic turbulence. *Journal of Fluid Mechanics* **812**, 991–1023.

Wang, G. & Richter, D. H. 2019 Two mechanisms of modulation of very-large-scale motions by inertial particles in open channel flow. *Journal of Fluid Mechanics* **868**, 538–559.

Wang, L. P., Ayala, O., G., Hui, A., C. & Mathews, K. L. 2014 Study of forced turbulence and its modulation by finite-size solid particles using the lattice Boltzmann approach. *Computers and Mathematics with Applications* **67**, 363–380.

Wang, L. P., Peng, C., Guo, Z. & Yu, Z. 2016 Flow modulation by finite-size neutrally buoyant particles in a turbulent channel flow. *Journal of Fluids Engineering* **138**, 041306.

Xia, Y., Lin, Z., Pan, D. & Yu, Z. 2021 Turbulence modulation by finite-size heavy particles in a downward turbulent channel flow. *Physics of Fluids* **33**, 063321.

Yeo, K., Dong, S., Climent, E. & Maxey, M. R. 2010 Modulation of homogeneous turbulence seeded with finite size bubbles or particles. *International Journal of Multiphase Flow* **36**, 221–233.

Yu, Z., Lin, Z., Shao, X. & Wang, L. P. 2017 Effects of particle-fluid density ratio on the interactions between the turbulent channel flow and finite-size particles. *Physical Review E* **96**, 033102.

Yu, Z., Xia, Y., Guo, Y. & Lin, J. 2021 Modulation of turbulence intensity by heavy finite-size particles in upward channel flow. *Journal of Fluid Mechanics* **913**, A3.

Zeng, L., Balachandar, S., Fischer, P. & Najjar, F. 2008 Interactions of a stationary finite-sized particle with wall turbulence. *Journal of Fluid Mechanics* **594**, 271–305.

Zhou, T., Zhao, L., Huang, W. & Xu, C. 2020 Non-monotonic effect of mass loading on turbulence modulations in particle-laden channel flow. *Physics of Fluids* **32**, 043304.